



Design and Development of Cost-Effective Equipment for Tribological Evaluation of Thermally Sprayed Abradable Coatings

K. Bertuol¹ · B. E. Arendarchuck¹ · F. R. E. Rivadeneira¹ · B. C. N. M. de Castilho¹ · C. Moreau¹ · P. Stoyanov¹

Submitted: 20 June 2024 / in revised form: 19 July 2024 / Accepted: 11 August 2024
© ASM International 2024

Abstract Thermally sprayed abradable coatings are essential for enhancing gas turbine engines' performance, as they are commonly used for clearance control purposes. Abradables act as protective barriers between the stationary casing and rotating blades. However, evaluating the abradability performance of novel coatings is challenging, because it is typically very costly and time-consuming. Thus, the goal of this project is to create a cost-effective test rig that can evaluate and pre-screen different thermally sprayed abradable coatings and understand how they interact with titanium blade tips under application-relevant conditions. The rig is capable of providing various inputs and outputs, including blade tip velocity, incursion rates, incursion depths, reaction forces, and interfacial temperatures. Aiming to validate the rig, a detailed dynamic evaluation was conducted, as well as abradability tests on aluminum, thermally sprayed polyester, and AlSi-

40Polyester abradable coating. The reaction forces for aluminum and polyester were overall higher when compared to AlSi-40Polyester. However, thermally sprayed polyester showed the highest interfacial temperatures of all materials tested. The difference in the reaction forces and interfacial temperature correlates well with the different wear mechanisms and thermal conductivities. Overall, the equipment showed to be a promising pre-screening methodology to evaluate and develop novel thermally sprayed abradable coatings.

Keywords abradability assessment · abradable coating · cost-effective equipment · pre-screening methodology · thermal spray

Introduction

Abradable materials are frequently used as clearance control elements within gas turbine engines, to reduce the gap between rotating and stationary components. Smaller gaps can lead to higher engine efficiency, reduced power loss, lower pollutant gas emissions, and environmental costs (Ref 1-3). However, achieving these benefits requires abradable materials to be removed smoothly by rubbing against a more abrasive moving material (e.g. blade), ensuring that the material wears while the abrasive part faces minimal wear (Ref 4).

The development of abradable coatings commonly involves thermal spray processes such as plasma spray, flame (combustion) spray, and high-velocity oxy-fuel (HVOF) (Ref 2, 5-7). Such coatings are desired to possess a relatively low hardness and elastic modulus, facilitating smooth rubbing without causing significant damage to the blade tips. Simultaneously, these coatings are also intended

This article is an invited paper selected from presentations at the 2024 International Thermal Spray Conference, held April 29–May 1, 2024, in Milan, Italy, and has been expanded from the original presentation. The issue was organized by Giovanni Bolelli, University of Modena and Reggio Emilia (Lead Editor); Fardad Azarmi, North Dakota State University; Sara Bagherifard, Politecnico di Milano; Partha Pratim Bandyopadhyay, Indian Institute of Technology, Kharagpur; Šárka Houdková, University of West Bohemia; Heli Koivuluoto, Tampere University; Yuk-Chiu Lau, General Electric Power (Retired); Hua Li, Ningbo Institute of Materials Technology and Engineering, CAS; Sinan Müftü, Northeastern University; and Filofteia-Laura Toma, Fraunhofer Institute for Material and Beam Technology.

✉ K. Bertuol
kaue.bertuol@mail.concordia.ca; kauebertuol@gmail.com

✉ P. Stoyanov
pantcho.stoyanov@concordia.ca

¹ Concordia University, Montreal, Quebec, Canada

to have a strong bonding strength as well as be resistant to corrosion and solid particle erosion. Balancing all these properties in a single material system is a considerable challenge, and thus, a typical abradable coating usually comprises three different phases: a matrix, solid lubricant, and binder (Ref 8-12). For instance, commercially available metallic abradables include aluminum–silicon–polyester, aluminum–silicon–graphite, nickel graphite, and nickel chromium aluminum–bentonite (Ref 13). Furthermore, innovative approaches take advantage of polymer properties, such as softness and corrosion resistance, which have led to robust abradable sealing coatings like AlSi + 40 wt.% polyester, aluminum–bronze–polyester, and MCrAlY-BN-polyester (Ref 14).

Despite substantial research on novel plasma-sprayed abradable coatings, their assessment is very challenging, especially regarding their wear resistance (Ref 10-12). Thus, only a few research groups focus on the wear mechanisms within abradable coatings–blade tip interactions and the interfacial process under application-relevant contact conditions (Ref 2, 14). Furthermore, by precisely assessing coating abradability under relevant conditions, high-speed abradable test rigs can lower evaluation costs by reproducing the rubbing processes in aero-engines on a smaller scale. This simulation replicates the conditions of a rotating blade inside a stator component to assess the wear and friction processes between abradable coatings and blade tips (Ref 14, 15).

Due to the importance of abradability evaluation on aero-engine applications, some research centers and companies have developed custom-made rig capabilities. A review of different testing rig facilities is discussed in the literature (Ref 16, 17). For instance, the Beijing General Research Institute of Mining & Metallurgy (BGRIMM) has developed a rig that contains a rotating disk with a single rectangular plate “bladelet” embedded radially in the circumference of the disk. The abradable is then moved at a specific speed into the rotating disk. The rig can be operated at a range of incursion rates and has the capability to introduce a hot gas to change the operating temperature of the rub. The rig is capable of measuring the rub forces through several force transducers. Similarly, NASA and Oerlikon Metco have developed abradable testing rigs, which have the capability to measure a wide range of rub forces and temperatures (Ref 17). In addition, the National Research Council Canada (NRC) has also developed a rig with the capability to have several bladelets installed in the rotating wheel instead of just one in the rig (Ref 18). More recently, a sophisticated rig has been developed at Ohio State University (OSU), which can reach representative engine diameters and speeds (Ref 19).

Although high-velocity abradable test rigs are effective, performing tribological assessments on abradable coatings

is still expensive and time-consuming. They are custom-made due to specific industrial requirements and testing conditions that are often kept confidential by aerospace and military entities. The complexity of these systems, which requires precise stability, advanced data acquisition, and stringent safety measures, contributes to their high cost (Ref 19-22). Consequently, abradability tests can exceed tens of thousands of dollars per condition, leading to limited data sets and restricting research to a comprehensive understanding of materials’ performance and conditions (Ref 23).

Thus, the primary objective of this research is to design and develop a cost-effective test rig method that can evaluate various thermally sprayed abradable coatings and their interactions with blade tips in an environment relevant to the aero-engine application. This cost-effective approach can significantly aid the tribological pre-screening of thermally sprayed coatings.

Design and Construction of a Cost-Effective Abradable Test Rig

Rig Overview

The cost-effective abradable test rig provides an efficient and inexpensive method to evaluate abradable coatings in a wide range of conditions. It is a low-risk, versatile, and cost-effective solution for abradable systems compared to other testing apparatus like high-speed abradable test rigs, test cells, on-wing, or in situ testing on operating turbine engines.

This rig aims to bridge the gap between low Technology Readiness Levels (TRL) using tribological tests (i.e., ball-on-flat and ball-on-disk) and high TRL with a dedicated high-speed abradable test rig. It allows a wide range of thermally sprayed materials to be tested under various conditions, primarily for pre-screening promising abradable materials before advancing to higher TRLs. This approach facilitates a thorough initial evaluation, helping to identify the most promising materials for further, more detailed, and expensive testing.

The newly designed abradable test rig offers numerous functional advantages, highlighted in Table 1. This rig excels in its ability to simulate diverse operational conditions with precision, ensuring reliable data acquisition crucial for optimizing abradable coating and blade performance. Its pre-screening approach facilitates early identification of optimal coating candidates, thereby enhancing efficiency in material assessment and scalability in industrial applications.

Critical aspects in validating different abradable systems include determining the rubbing reaction forces, and

Table 1 Key advantages of the cost-effective abradable test rig

Advantage	Description
Cost-Efficiency	Significantly reduces expenses for tribological evaluations, making testing more accessible (e.g., conducting multiple abradable coating tests within limited resources)
Versatility	Able to accommodate different blades and abradable materials at different conditions (i.e., blades with different geometries and thickness-to-chord ratios)
Laboratory Simulation	Capable of simulating gas turbine engine conditions with precise control over key parameters
High-Resolution Data Acquisition	Provides detailed measurements of critical parameters like reaction forces and temperature (e.g., monitoring force fluctuations at each 5 microseconds)
Reliability and Repeatability	Ensure reliable experiments with reproducible and precise control (e.g., consistent wear behavior in repeated tests)
Early Issue Detection	Allows early identification of potential coating issues, facilitating prompt adjustments (e.g. detecting premature coating failure under specific conditions)
Comparative Analysis	Enables side-by-side comparisons of different coatings under identical conditions (e.g., evaluating performance between different material compositions or blade materials)
Validation of Coating Performance	Offers a platform for validating performance and optimizing spray parameters and material selection (e.g. pre-screening optimal spray parameters in terms of abradability performance)
Wide Range of Operational Conditions	Accommodates various operational conditions to mimic different real-world scenarios (e.g., testing the effects of varying incursion rates on coating wear)
Adaptable for Scaling Up to Higher TRL	Facilitates transition to higher TRL for broader industrial and research applications, enabling larger-scale industrial testing to meet enhanced operational and performance criteria.

Table 2 Inputs and outputs of the abradable test rig and their descriptions and range of operation

Input parameter	Description	Range
Blade speed	The linear speed of the blade tip at its outermost edge	0–60 m/s
Incursion rates	The rate at which the blade penetrates the abradable material	5–500 μm/s
Incursion depths	The maximum depth of blade incursion into the abradable material	0–5 mm
Operating temperature	The operating temperature of the abradable material and the blade	Room Temperature
Output parameter	Description	Range
Reaction forces	The resultant rubbing forces created by the blade-abradable interaction	Up to 30 kN
Interfacial temperature	The localized temperatures generated during blade-abradable contact	Up to 1200 °C
Blade wear	The measurement of material loss or degradation of the blade	–
Transfer	The material transfer from the abradable coating to the blade	–
Wear mechanism	The study of the mechanisms by which wear occurs at the blade-abradable interface	–
Debris characteristics	Analysis of debris generated during blade-abradable interactions	–

frictional heating temperatures, as well as identifying wear mechanisms and blade wear under various operating conditions (Ref 11, 24). Therefore, the custom-built abradable test rig offers a wide scope of inputs and outputs.

Table 2 outlines the abradable test rig’s main inputs and outputs, along with their corresponding descriptions and operational ranges. These inputs and the rig’s adaptiveness allow testing over a wide range of conditions, which can play a crucial role in simulating real application scenarios

to evaluate the performance of turbine blade systems. In addition, the outputs obtained from the abradable test apparatus play a significant role in understanding and optimizing the performance of abradable materials and turbine blade systems.

It should be noted that the main limitation of the cost-effective abradable rig is its restricted blade speed, which is capped at 60 m/s. This is notably lower compared to the typical high-speed abradable rig, which can reach speeds of

300 m/s or even 500 m/s in certain instances (Ref 11, 18, 25–27). Nevertheless, this testing setup is essential for pre-screening candidate material compositions and evaluating actual sprayed abrasible coatings, facilitating the optimization of spray parameters. A few authors also investigated the blade-abrasible interaction using simplified setups, such as ballistic bench (Ref 28, 29), scratch test (Ref 30), pin-on-disk (Ref 31, 32), single-pass pendulum scratch test (Ref 27), and adapted high-speed milling machine (Ref 33). Each of these simplified setups has its limitations, varying in terms of speed, geometry, and aero-engine representativeness.

Figure 1 presents a schematic representation of the blade-abrasible interaction. It shows the movement of the abrasible coating toward the rotating blade, resulting in material removal, adhesive transfer to the blade tip, and debris formation. Additionally, it highlights some of the key input parameters for the system, such as the incursion movement and depth. The incursion movement refers to the horizontal motion of the abrasible material, allowing the blade tip to penetrate into the material and start rubbing.

Mechanical Layout

Using SolidWorks 3D software, a model of the full equipment was designed, and it is presented in Fig. 2. The testing apparatus can be divided into rotational and linear stages. Regarding the rotational stage, a rotating disk is connected to a motor providing high tangential speed during testing. In addition, a dummy blade tip can be mounted on the disk to simulate a rotating blade in a real application environment in an aircraft turbine (see Fig. 2b and 2c). The three-dimensional modeling was generated to visualize the ultimate product and fine-tune the components before the commencement of physical production.

In terms of the blade tip geometry, an equivalent simplified geometry was proposed to mimic the rotor blade-casing interaction. The cost-effective abrasible test rig was

designed to accommodate several configurations depending on the target thickness-to-chord ratio (t/c) of relevant application scenarios, as seen in Fig. 2c. In the custom-built abrasible test rig, the chord can range between 5 and 15 mm, and the thickness can range between 0.5 and 4 mm. These values were selected based on conventional blading techniques proposed by Saravanamuttoo (Ref 34), which suggests a t/c ratio of 0.1 up to 0.2. Similarly, Kacker and Okapuu (Ref 35) and Moustapha and Zelesky (Ref 36) suggest a typical t/c ratio for a blade cross section ranging between 0.13 and 0.32.

In terms of the specimen size dimensions of the abrasible coating, the mechanical design of the sample holders was engineered to accommodate flat samples with a width ranging from 20 mm to 30 mm and a thickness from 2 mm to 10 mm. Since the samples are flat, the length of the sample is directly related to the expected length of the rubbing wear track, which is associated with and limited by the maximum incursion depth (Ref 37, 38). Typically, abrasibility tests are conducted with incursion depths ranging from 0.4 mm to 2 mm (Ref 27, 38, 39). Considering the blade's rotational radius (300 mm), the suggested length of the flat samples varies from 40 to 95 mm, ensuring additional dimensions for safety.

In order to establish a cost-effective and reliable approach for evaluating thermally sprayed abrasible coatings, the apparatus was constructed through the integration of mechanical and electronic components, such as a rotor, linear guide, stepper motor, and planetary gearbox. For the rotor, the King KWL-1218VS lathe was selected for its capacity to vary rotational speed up to 3,800 rpm (equivalent to 63.3 Hz) and a swing-over bed of 305 mm. Figure 3a illustrates a photograph of the lathe. In addition, a 300-mm-diameter stainless disk was machined and attached to the headstock, resulting in a linear blade speed of 60 m/s due to the combination of lathe speed and disk diameter.

A linear slide module integrated with a gear box, stepper motor, and sample holder was engineered to provide the linear movement of the abrasible material. This setup facilitates the blade insertion process into the sample, emulating real-world rubbing scenarios. To achieve a range on incursion rate from 5 to 500 $\mu\text{m/s}$, a custom-built GX120-2505-200 linear guide model equipped with 2 trolleys was designed (Fig. 3b). Also, a commercially available NEMA 34 stepper motor (generating 12 Nm) and a 100:1 planetary gearbox were selected and attached to the movable specimen stage. This choice was based on considerations of precision and the extensive range achievable through the collaboration of a linear guide module and a stepper motor.

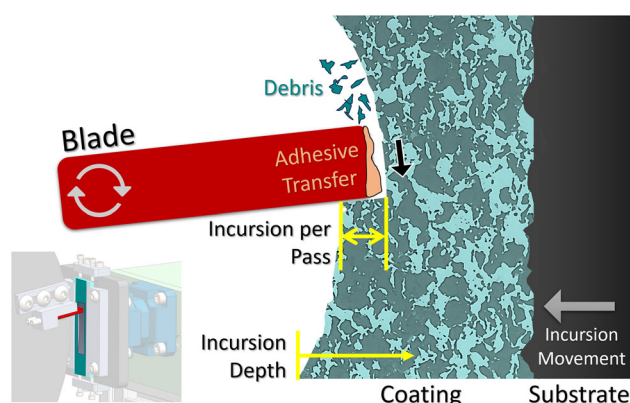


Fig. 1 Schematic of the abrasible test

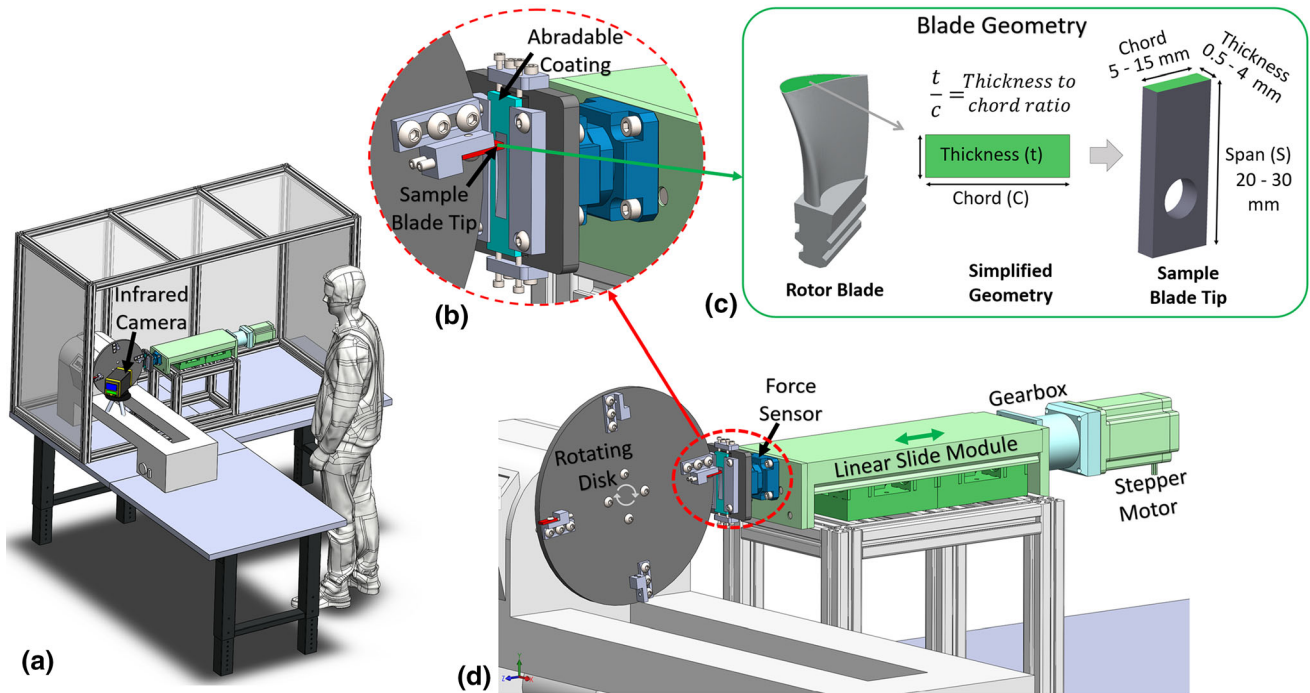
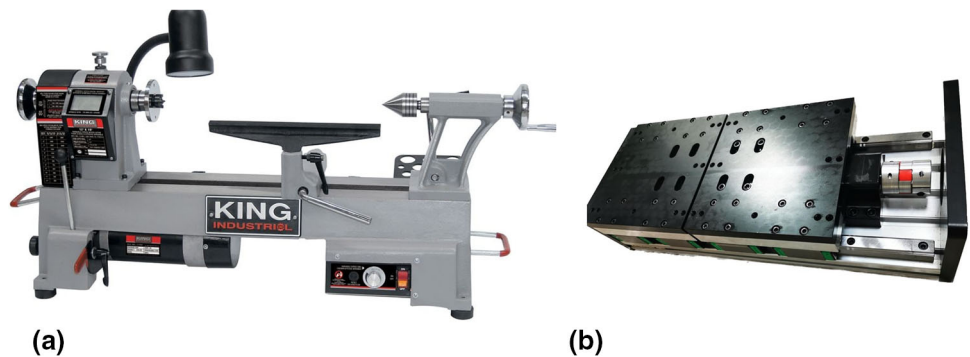


Fig. 2 3D modeling of the cost-effective abrasible test rig. (a) Overview of the equipment, (b) close view of the abrasible coating and blade mounted, (c) simplified sample blade tip geometry, (d) detailed view of the movable specimen stage and rotating disk

Fig. 3 (a) Wood lathe model King KWL-1218VS, (b) linear guide module model GX120-2505-200, (c) stepper motor Nema 34, (d) planetary gearbox 100:1



Instrumentation and Data Acquisition

The device in Fig. 4a, identified as a triaxial load cell Kistler 9347C, is a piezoelectric force transducer designed to accurately measure all forces acting on the three orthogonal components in any direction. The load cell is installed between two plates with preload and can measure both normal and tangential forces acting on the abrasible coating during the test. Utilizing the piezoelectric principle, a force generates an electric charge that enables simple, direct, and highly accurate measurements. For the measurement signal processing, a Kistler LabAmp Laboratory Charge Amplifier quasi-static, model 5167A (Fig. 4b) is essential for converting the measurement signal into an electrical voltage and facilitating comprehensive reaction force measurement (Ref 40, 41).

The combined instrumentation system of the load cell and amplifier possesses a sampling capability of 200 kSps (kilo samples per second) per channel (Ref 40), far exceeding the necessary data measurement requirements. Considering the inverse relationship between frequency and period, this system can extract data every 5 microseconds. This sampling rate is approximately 3000 times higher than the period between each impact, which is 17 milliseconds considering the rig’s rotational speed (i.e., up to 3000 data points can be acquired between each full blade revolution). Detailed frequency analysis and validation of this system are elaborated on and discussed in the section “Data Acquisition and Rig Validation”.

In order to accurately measure the surface temperature of the abrasible coating during the abrasibility tests, an A320 ThermoVision infrared camera (FLIR Systems, MA)

Fig. 4 (a) Triaxial load cell model Kistler 9347C, (b) laboratory amplifier model Kistler LabAmp 5167A, (c) FLIR A320 ThermoVision infrared camera, (d) programmable controller model ST-PMC1

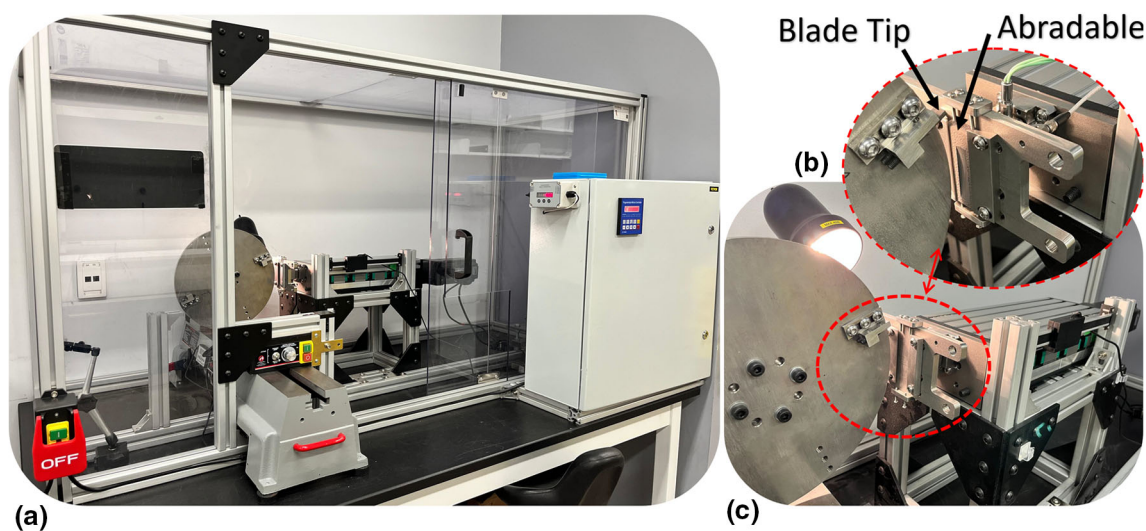
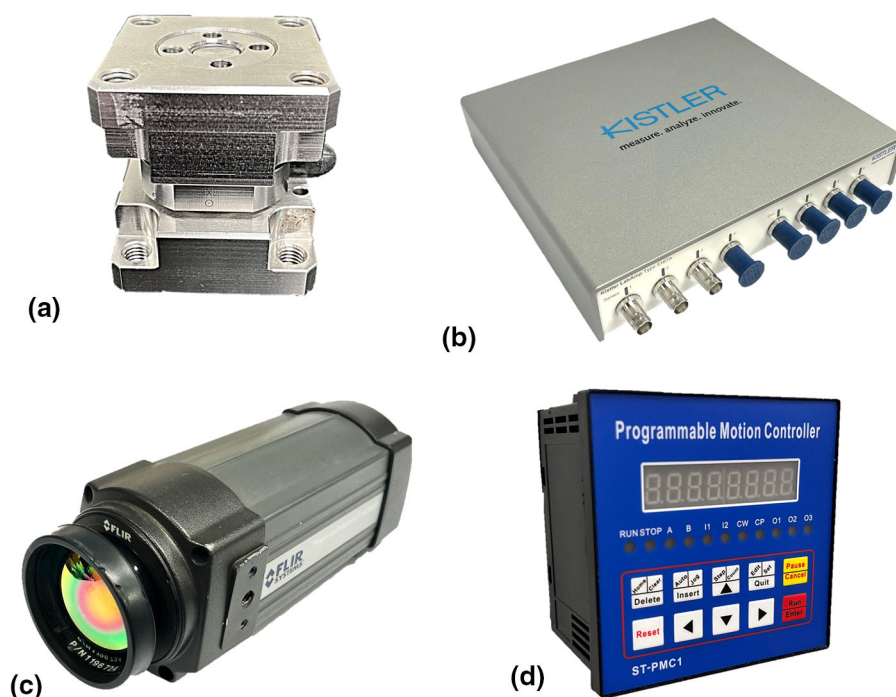


Fig. 5 (a) Overview of the cost-effective abrasion test rig, (b) abrasion coating mounted on the sample holder, (c) close view of the disk and moveable specimen stage

(Ref 42) was integrated into the test rig. This infrared camera (Fig. 4c) is calibrated to detect temperature variations within the range of 0 to + 350 °C, maintaining an accuracy of ± 2 °C. The camera system is equipped with a dynamically updated reference temperature to ensure precise monitoring. Although the setup is designed to monitor the overall interfacial temperature (e.g., caused by friction heating) of the coating over time, the camera's detector has a response time of 12 milliseconds, enabling real-time temperature monitoring and data extraction between each

impact period. These measurements, combined with the incursion rate, can be accurately converted and associated with the rubbing depth during the abrasion tests, providing a comprehensive understanding of the overall rubbing temperature evolution. Before testing, parameters such as material emissivity, measurement distance, and required data accuracy must be known and adjusted.

In addition, several electronic devices were carefully chosen to allow flexible adjustment of the incursion rate, such as control and monitor the movable specimen. These

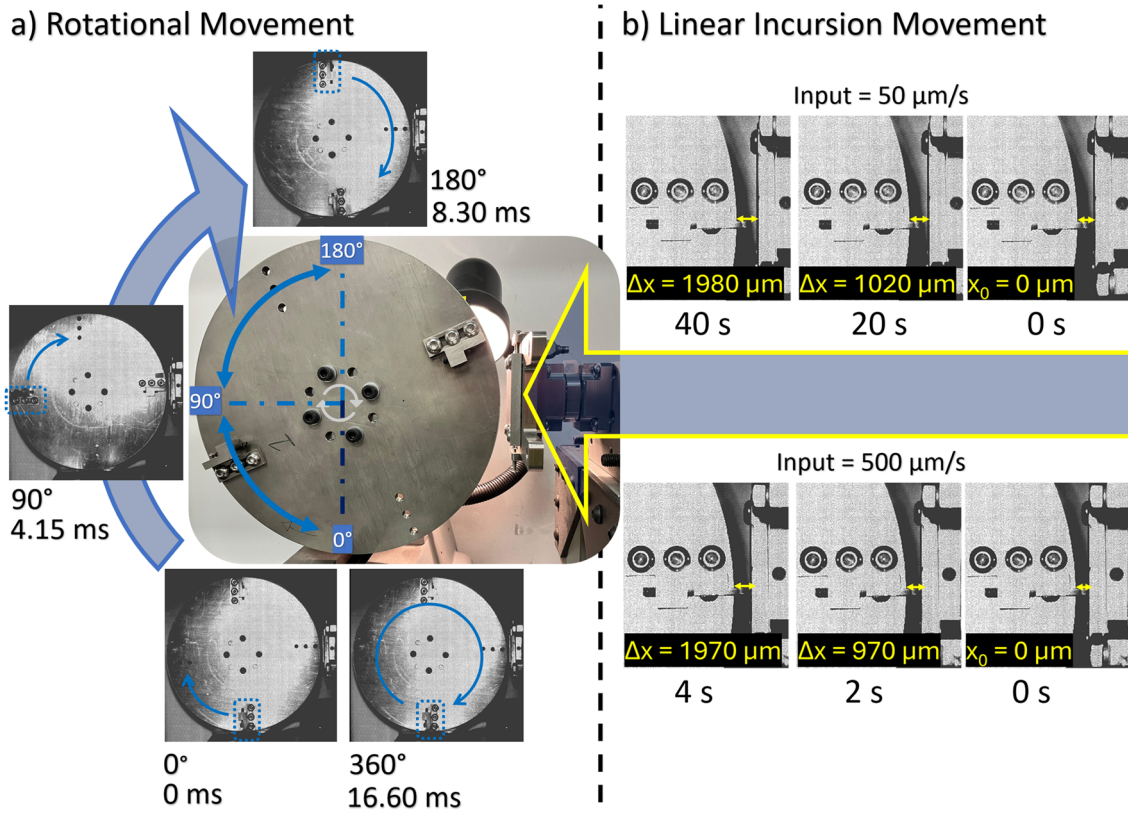


Fig. 6 Investigation of the system dynamics at 3600 rpm and at two different incursion rates. (a) Evaluation of the rotating speed using high-speed camera imaging. (b) Analysis of the linear incursion movement at 50 $\mu\text{m/s}$ and 500 $\mu\text{m/s}$ using high-speed camera imaging

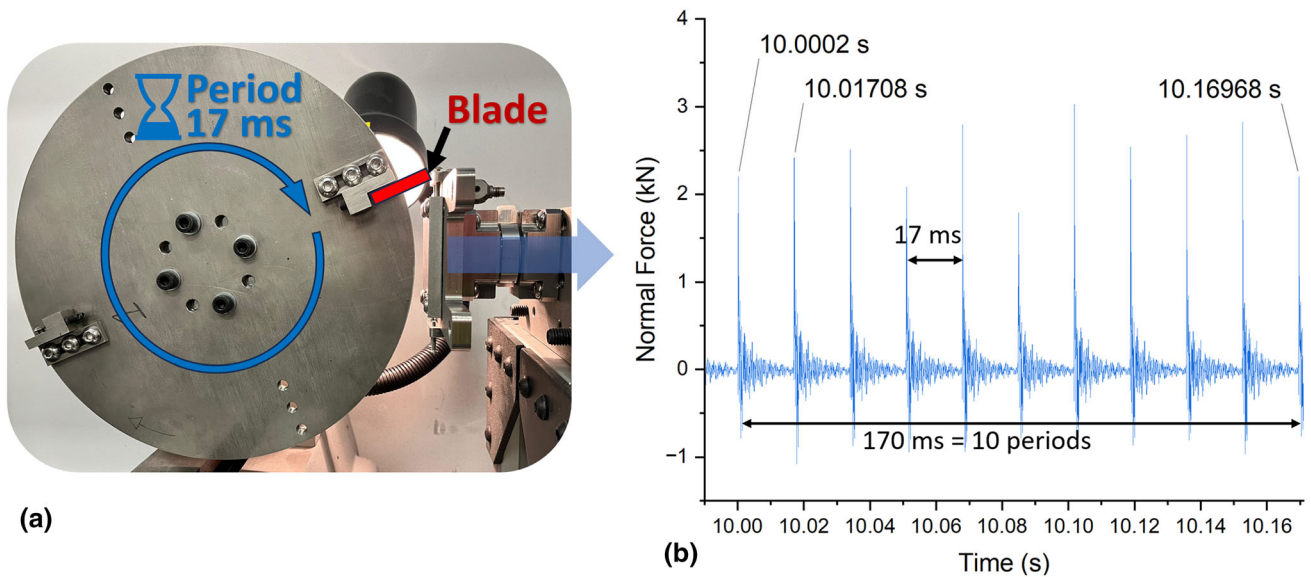


Fig. 7 Evaluation of the blade impact period during testing. (a) Side view of the abrasion test rig, illustrating the theoretical blade impact period, (b) plot of normal reaction forces over time, showing the observed blade impact periods during the test

devices include a CNC Servo Driver model 2HSS86 that connects to the stepper motor and the Stepper Motor Programmable Controller model SainSmart ST-PMC1 (Fig. 4d) (Ref 43). Two adjustable power supplies with a

capacity of 480W and a voltage range of 0–48 V were also selected to provide power to the system. Additionally, a digital readout kit was integrated into the moveable stage

Table 3 Abradable test parameters

Abradable test parameters	Description	Value	Unit
Blade and abradable characteristics	Blade material	Ti6Al4V (Grade 5)	...
	Sample dimensions	25 × 76	(mm)
	Rubbing surface (blade contact area)	10 × 3.18 mm = 31.8	(mm ²)
Input parameters	Blade speed	50	(m/s)
	Incursion rate	50 (0.83 μm/pass)	(μm/s)
	Incursion depth	1500 & 2000*	(μm)
Extras	Disk rotation	3600	(rpm)
	Operational temperature	Room temperature	(°C)
	Humidity	20%	...

*AlSi-40Polyester (2000 μm); polyester coating and aluminum sheet metal (1500 μm)

to facilitate precise monitoring of the incursion depth by the operator during the test.

Manufacturing and Assembly

In pursuit of the rig's optimal functionality, machining techniques were applied to fabricate minor components crucial for interconnecting various rig devices. Key concerns included stability, balancing, and the management of static and dynamic loads under operational conditions. The list of components includes the rotating disk, sample holders, joints, and supports. The rotating disk was laser-cut and machined to ensure precise weight and geometric distribution, as well as the blade sample holders that were uniformly distributed to balance the mass. This careful engineering ensures smoother operation by minimizing vibrations and enhancing the reliability of experimental results.

In addition, aluminum extrusion profiles were also employed to facilitate joining and support for the mechanical assembly. To enhance operational safety, a protective case was fabricated, featuring a covering composed of a 6 mm-thick bullet-resistant polycarbonate sheet (Lexan, GE). This material was selected since it exhibits high impact strength and heat resistance, making it suitable for severe dynamic impact and thermal loads (Ref 44). A few ballistic tests have already proven the efficiency of the polycarbonate under both normal and inclined dynamic impacts (Ref 45-47). Among those, Radin and Goldsmith (Ref 47) performed bullet tests at 82.1 m/s and 93.9 m/s against polycarbonate plates with similar thicknesses.

The fully assembled cost-effective abradable test rig is illustrated in Fig. 5a. A more detailed perspective of the sample holder, showcasing the mounted abradable coating before initiating the test, is presented in Fig. 5b.

Additionally, Fig. 5c exhibits the assembled movable specimen stage.

Data Acquisition and Rig Validation

Dynamics Evaluation

A detailed investigation, especially in terms of dynamics, was conducted to provide insights into the performance and reliability of the abradable test rig under operational conditions. To validate the accuracy of rotational speed, linear incursion position, and incursion rate, a high-speed camera (Model HSI FASTCAM SA1.1) (Ref 48) was used to monitor the position over time at 20000 fps. Thereby, qualifying the dynamic mechanism system, such as the lathe and the ST-PMC1 programmable controller inputs (e.g., rpm, and incursion rate). Figure 6 is a visual representation of the methodology and results mentioned.

For the linear incursion movement analysis, images were captured at specified time intervals (as depicted in Fig. 6b), and the position of each was measured to confirm the incursion rate input and system stability. A comparable approach was utilized for the rotational movement analysis (Fig. 6a). In this case, four distinct positions were selected, and the time interval required to move between them was observed to verify the rotational speed. The data indicated that both the linear and rotational movements were within the expected operational range, confirming the accuracy of the input parameters and the stability of the system. This comprehensive validation underscores the reliability and precision of the test rig's dynamic performance under operational conditions.

Given the rig's rotational speed input of 3600 rpm, resulting in an impact frequency of 60 Hz and, consequently, an impact interval of about 17 milliseconds

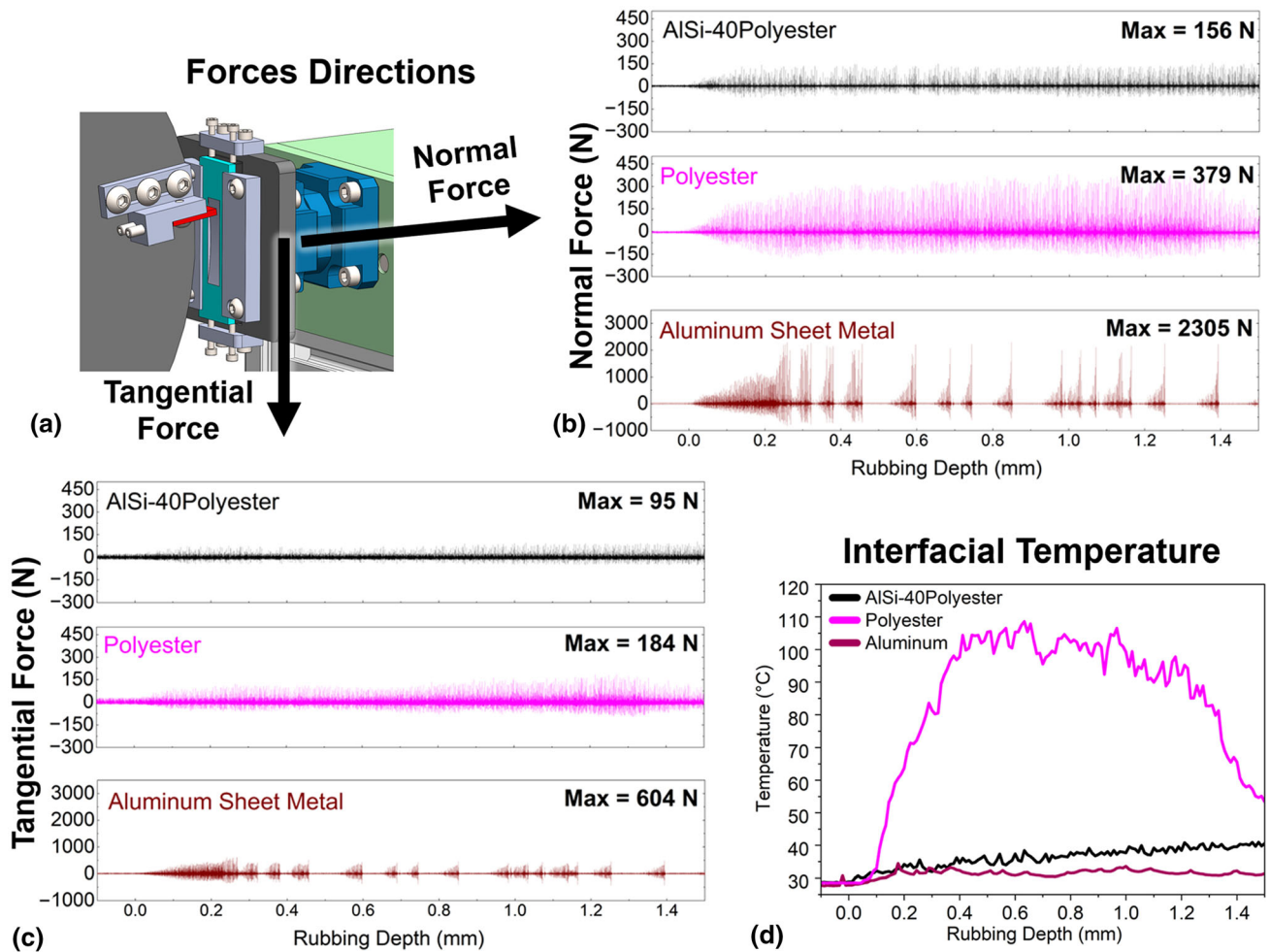


Fig. 8 Reaction forces and interfacial temperatures along the rubbing depth. (a) Schematic illustrating the direction of the reaction forces, (b) normal force of AISi-40Polyester (Ref 50), polyester, and

aluminum sheet metal, (c) tangential force, (d) interfacial temperature of the three materials during the abrasability test. Reprinted from Ref 50, available under CC BY-NC 4.0 license at ScienceDirect

between each full blade rotation, a comprehensive investigation was conducted. This investigation aimed to establish a practical and theoretical correlation to qualify the natural frequency and direct impact forces. Kistler Triaxial Accelerometer model 8763B500 (Ref 49) alongside the data acquisition force system was used to qualify the dynamics impact during tests and compare with the theoretical impact frequency. Figure 7 illustrates the main results, demonstrating that the data align with the anticipated acquisition range, showing a peak every 17 milliseconds (first touch point). These findings confirm the rig’s accuracy, ensure the natural frequency of the rig outside the operational range, and validate the reliability of the force acquisition system.

Materials Testing

Aiming to validate the abrasable test rig in terms of materials pre-screening, three different materials were

tested. The first material was a conventional thermally sprayed abrasable material AISi-40Polyester, and due to its significance as an abrasable coating, three tests were performed on this material. More details on the spraying equipment and parameters can be found elsewhere (Ref 50-52). In addition to the validation process, a thermally sprayed polyester and a conventional aluminum sheet metal were also selected since they are the primary elements found in traditional aluminum–silicon–polyester abrasable coatings. This selection was made to facilitate comparative analyses and ensure a comprehensive evaluation of the performance and characteristics of the abrasability testing. The tested parameters used on all samples can be found in Table 3.

Reaction Forces and Temperatures

The normal and tangential forces during rub are commonly used to analyze the abrasability properties of thermally

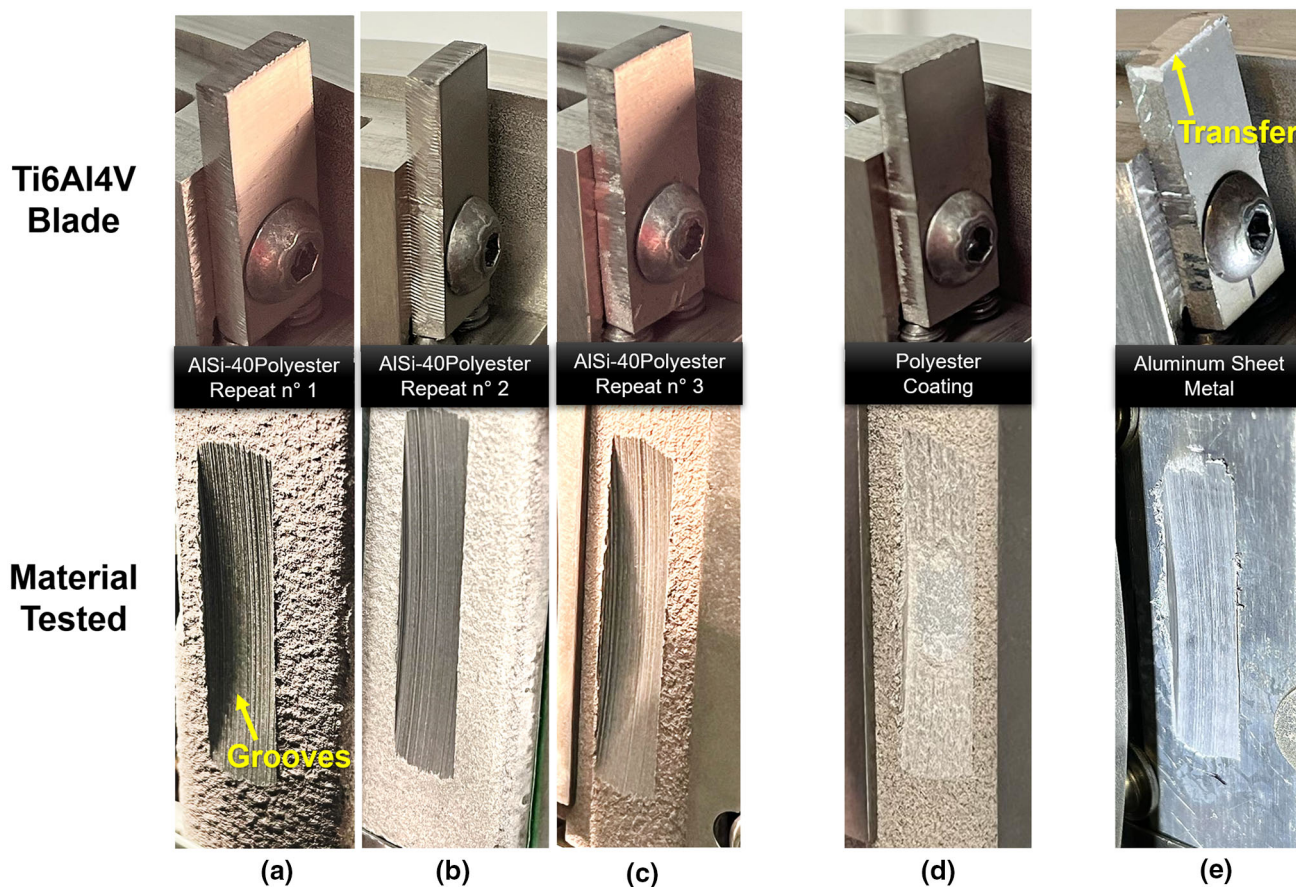


Fig. 9 Different materials tested in the cost-effective abrasible test rig. (a) AlSi-40Polyester, repeat number 1 (Ref 50), (b) AlSi-40Polyester, repeat number 2, (c) AlSi-40Polyester, repeat number 3,

(d) thermally sprayed polyester, (e) aluminum sheet metal. Reprinted from Ref 50, available under CC BY-NC 4.0 license at ScienceDirect

sprayed abrasible materials (Ref 24, 37), and minimal rubbing reaction forces are desired in order to protect the blade (Ref 22, 50). Figure 8b and 8c presents the reaction forces acting on the specimens during their respective rubbing tests. It should be noted that for comparison reasons, Fig. 8 only presents results up to 1500 μm , despite the incursion depth of the AlSi-40Polyester sample being performed up to 2000 μm . Other specimens, such as polyester coating and Al sheet metal, were tested up to 1500 μm incursion depth due to safety concerns related to the available thickness of the samples. The normal and tangential forces for AlSi-40Polyester were evidently lower compared to the aluminum and polyester. Indeed, the AlSi-40Polyester was specifically designed to be an effective abrasible.

Both thermally sprayed coatings, AlSi-40Polyester and polyester demonstrated consistent and effective cutting, as evidenced by the uniform distribution of forces throughout the rubbing depth (Fig. 8b and 8c). Similarly, Zhang et al. (Ref 15) measured the reaction forces of AlSi-Polyester against Ti6Al4V blades using a comparable incursion rate (50 $\mu\text{m/s}$), noting a cycle forces pattern with peaks similar

to the force behavior presented in this study (see Fig. 8b and 8c).

In a quantitative evaluation, AlSi-40Polyester exhibited the lowest reaction force (156 N), which was almost 2.5 times lower than that of the polyester material. These results are close to the ones available in literature using other custom-made abrasible rigs, even using distinct cutting characteristics. Recently, Zhang and Marshall (Ref 37) observed equivalent reaction forces in a range of about 100 N and rubbing temperatures of about 200°C on tests using a different high-speed abrasible test rig, by means of a knife-edge methodology on coatings with similar chemical compositions.

On the other hand, the aluminum sheet metal tested as denser and harder material exhibited numerous ruptures and non-uniform cutting, leading to larger chips, higher maximum reaction forces (2305 N), and discontinuous loads.

Figure 8d shows the interfacial temperature for the three materials tested as a function of the rubbing depth. AlSi-40Polyester exhibited a steady increase in temperature, reaching a maximum of 44 °C at the maximum incursion

depth. Similar investigations have explored the interfacial temperature in abradable coatings and its association with friction forces (Ref 11, 26, 53). Additionally, the results observed by Watson and Marshall (Ref 54) performed on a different abradable rig indicated that the peak temperature was achieved using 0.2 $\mu\text{m}/\text{pass}$ (below 200 °C), which was close to the 0.83 $\mu\text{m}/\text{pass}$ used in the current study.

On the other hand, the interfacial temperature for the thermally sprayed polyester was significantly higher, reaching up to 109°C. However, for the aluminum, the maximum temperature was 35°C, which is lower than the temperatures on AlSi-40Polyester tests. This can be attributed to its higher thermal conductivity and non-continuous cutting, which helped to lower the heat generated during the rubbing.

Similarly to the findings in this validation process, many studies observed equivalent outcomes that can be associated with reaction forces, including rougher scar appearance (Ref 18), adhesive transfer (Ref 27), and blade wear (Ref 22).

Coating and Blade Analyses

The AlSi-40Polyester abradable coating presented a clean and smooth cut in all tests (Fig. 7b, 7c, 9a), indicating a consistently good abradability of the coating and high stability of the apparatus. This can be observed by the

shallow grooves on the rubbing wear track (see Fig. 9), which is associated with the expected dominant abrasive wear mechanism. This is consistent with previous studies on thermally sprayed abradable coatings, which showed similar wear tracks (Ref 24, 37, 55).

The tests performed on aluminum sheet metal showed a significantly higher adhesive transfer to the titanium blade due to aluminum’s high chemical affinity (Ref 56) and its higher metallic content compared to the abradable coating AlSi-40Polyester. As observed in literature (Ref 55, 57), a higher concentration of aluminum typically leads to a higher adhesive transfer, as shown in Fig. 9e. This feature also explains the increased reaction forces observed in Fig. 8, which were driven by a higher contribution of aluminum’s adhesive transfer to the blade and the fact that aluminum sheet metal was a denser and bulk material.

Moreover, several research groups have observed similar wear behaviors on different abradable test rigs. Mutasim et al. (Ref 58) conducted an abradability evaluation of Al-based coatings, comparing them with other abradables and pure aluminum against a 4043 steel blade. Their results indicated no coating debonding, chipping, or smearing, with clean and uniform groove cuts observed. At the same time, aluminum samples did not perform well in the abradability tests, similar to the findings of the rig used in this study.

In order to elucidate the effective cutting of the AlSi-40Polyester abradable coating in the cost-effective

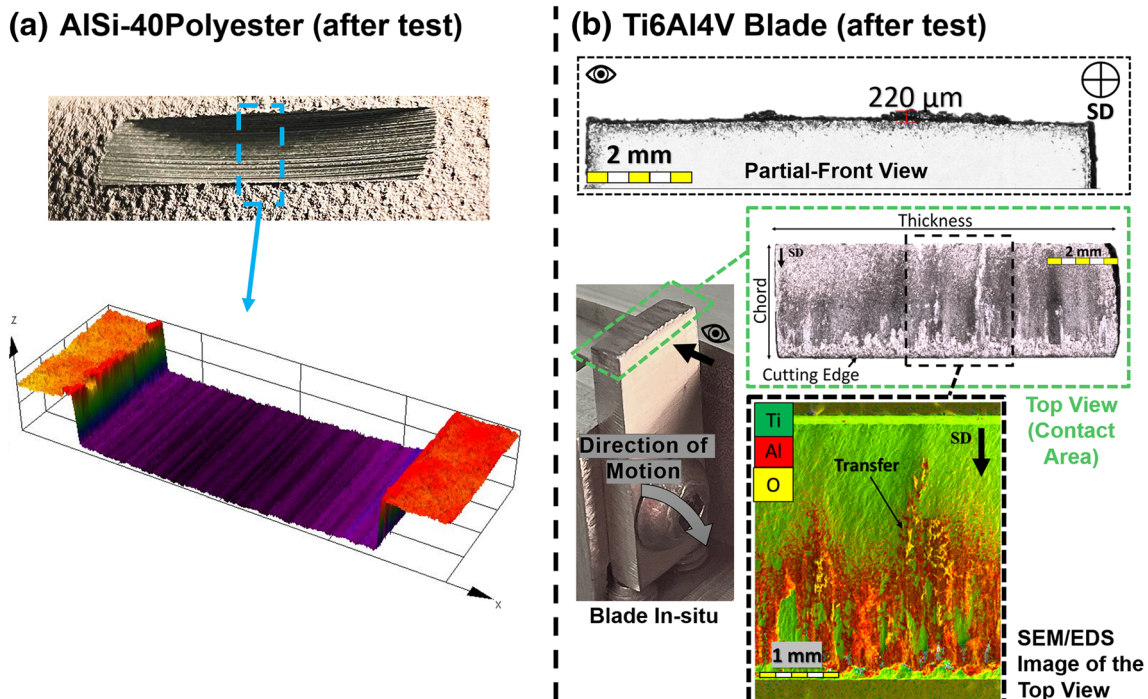


Fig. 10 (a) Photograph and 3D microscopical image of AlSi-40Polyester wear track after rubbing test, (b) Ti6Al4V blade images and elemental mapping after rubbing test (Ref 50). Reprinted from Ref 50, available under CC BY-NC 4.0 license at ScienceDirect

abradable rig, the samples were investigated in more detail in terms of wear and adhesive transfer. Figure 10a shows a 3D microscopical image of the wear track of the rubbed abradable material. The worn surface exhibits grooves produced by the abrasive wear mechanism parallel to the direction of motion.

Similarly, Zhang et al. (Ref 15), when carrying out tests at 350 °C using a high-speed abradable test rig, showed that the blades also formed parallel grooves on the coating with similar cutting behavior. Using a different abradable test rig, Liu et al. (Ref 55) also observed groove formation in the coatings without debonding, with regular-shaped wear tracks and relatively smooth surfaces, consistent with the findings from the rig developed in this current study.

Meanwhile, in Fig. 10b, the Ti6Al4V blade tip used against the AlSi-40Polyester reveals no wear on the blade. However, as found by some authors (Ref 8, 10, 59, 60), the blade showed the evident formation of a transfer film, which can be seen on the front and top view (see Fig. 10b). This adhesive transfer film was predominantly formed by the aluminum from the abradable coating to the blade.

An equivalent adhesion mechanism was also observed by Rahimov et al. (Ref 60). They tested the AlSi-Polyester coating against Ti6Al4V blades and found parallel groove formation in the coating when analyzed at a close blade speed (85 m/s), corroborating the previous discussion's results. These results reinforce the reliability of the conclusions and data acquired from the cost-effective abradable test rig compared to other abradable test rigs.

Conclusions

In this study, a cost-effective abradable test rig was designed to pre-screen thermally sprayed abradable systems. This setup provides valuable insights into the interaction between abradable coatings and blade tips and their wear behavior. Its ability to simulate operational conditions, adapt different materials, and take a prompt, cost-effective approach is crucial for enhancing the efficiency of material assessment.

In order to validate the rig, a detailed dynamic evaluation was conducted to provide insights into the performance and reliability of the abradable test rig under operational conditions. In addition, two thermally sprayed materials (AlSi-40Polyester and polyester) and a commercial aluminum sheet metal were investigated. The AlSi-40Polyester presented the lowest reaction forces with no significant blade wear. In addition, the polyester coating showed significantly higher interfacial temperature, which can be attributed to its low thermal conductivity. The tests performed on the aluminum sheet metal, on the other hand,

presented significantly higher adhesive transfer on the blade and the highest reaction forces.

Moreover, a comprehensive understanding of the rig's design and setup can significantly benefit other research groups by serving as a reference for developing similar test rigs. This can foster consistency and comparability across different studies, facilitating advancements in the field. Detailed documentation of our rig's validation process can help other researchers replicate our setup, adapt it to their specific needs, and ultimately contribute to a broader and more reliable body of knowledge within the community. Such collaborative progress is essential for pushing the boundaries of fields such as tribology and thermal spray, which can be a powerful ally when pre-screening new thermally sprayed candidate coatings for abradable systems.

References

1. U. Rathmann, S. Olmes, and A. Simeon, Sealing Technology: Rub Test Rig for Abrasive/Abradable Systems, *Volume 5: Turbo Expo 2007*, (Montreal, Canada), ASME, 2007, p 223-228, <https://doi.org/10.1115/GT2007-27724>.
2. M.R. Dorfman, G. Dwivedi, C. Dambra and S. Wilson, Perspective: Challenges in the Aerospace Marketplace and Growth Opportunities for Thermal Spray, *J. Therm. Spray Technol.*, 2022, **31**(4), p 672-684.
3. P. Stoyanov, K.M. Harrington and A. Frye, Insights into the Tribological Characteristic of Cu-Based Coatings Under Extreme Contact Conditions, *JOM*, 2020, **72**(6), p 2191-2197.
4. M.W. Smiarowski, R. Leo, C. Scholten, and J. Blake, Steam Turbine Modernization Solutions Provide a Wide Spectrum of Options to Improve Performance, *Siemens Power Generation*, 2005.
5. Oerlikon Metco, Atmospheric Plasma Spray Solutions, 2022.
6. L. Pawłowski, *The Science and Engineering of Thermal Spray Coatings*, 2nd ed. Wiley, Chichester, 2008.
7. S. Wilson, Abradable Thermal Spray Applications and Technology, *Thermal Spray Technology*, R.C. Tucker, Ed., ASM International, 2013, p 287-295, <https://doi.org/10.31399/asm.tb.v05a.a0005738>.
8. M. Bounazef, S. Guessasma and B. Ait-Saadi, The Wear, Deterioration and Transformation Phenomena of Abradable Coating BN-SiAl-Bounding Organic Element, Caused by the Friction between the Blades and the Turbine Casing, *Mater. Lett.*, 2004, **58**(27-28), p 3375-3380.
9. C.U. Hardwicke and Y.-C. Lau, Advances in Thermal Spray Coatings for Gas Turbines and Energy Generation: A Review, *J. Therm. Spray Technol.*, 2013, **22**(5), p 564-576.
10. F. Mohammad, M. Mudasar and A. Kashif, Criteria for Abradable Coatings to Enhance the Performance of Gas Turbine Engines, *J. Mater. Sci. Metall.*, 2021, **2**(1), p 101.
11. E. Irissou, A. Dadouche and R.S. Lima, Tribological Characterization of Plasma-Sprayed CoNiCrAlY-BN Abradable Coatings, *J. Therm. Spray Technol.*, 2014, **23**(1-2), p 252-261.
12. N. Fois, M. Watson and M. Marshall, The Influence of Material Properties on the Wear of Abradable Materials, *Proc. Inst. Mech. Eng. Part J. J. Eng. Tribol.*, 2017, **231**(2), p 240-253.
13. Oerlikon Metco, Thermal Spray Materials Guide, 2015.

14. Oerlikon Metco, Thermally Sprayed Abradable Coating Technology for Sealing in Gas Turbines, (Brussels, Belgium), 6th International Conference, 2012.
15. N. Zhang, J. Shen, H. Xuan, Y. Hu and W. Hong, Evaluation of an AlSi-Polyester Abradable Seal Coating Performance Using High-Temperature and High-Velocity Abrasion Tests, *Proc. Inst. Mech. Eng. Part J. J. Eng. Tribol.*, 2016, **230**(7), p 842-851.
16. K. Bertuol, F. Rivadeneira, R. Nair, C. Moreau, and P. Stoyanov, Advancing Abradable Evaluation: A Comprehensive Review and Development of an Innovative Cost-Effective Methodology, (Presented at the 27th International Congress of Mechanical Engineering, COBEM 2023, Florianopolis, Santa Catarina, Brazil), 2023.
17. Q.Y. Lu, J. Shen, Y.G. Yu, X.J. Ren, H.J. Xuan and T. Liu, Progress on Facilities and Methodology to Evaluate Abradable Seal Coatings, *Adv. Mater. Res.*, 2013, **690-693**, p 1992-1998.
18. A. Dadouche, M.J. Conlon, W. Dmochowski, B. Liko, and J.-P. Bedard, Experimental Evaluation of Abradable Seal Performance at High Temperature, *Volume 5: Structures and Dynamics, Parts A and B*, (Berlin, Germany), ASMEDC, 2008, p 143-150, <https://doi.org/10.1115/GT2008-51228>.
19. Padova, Jeffrey Barton, Michael G. Dunn, Steve Manwaring, Gamaliel Young, Maurice Adams, and Jr. Michael Adams, Development of an Experimental Capability to Produce Controlled Blade Tip/Shroud Rubs at Engine Speed, *J. Turbomach.*, 2005.
20. H. Ma, F. Yin, Y. Guo, X. Tai and B. Wen, A Review on Dynamic Characteristics of Blade-Casing Rubbing, *Nonlinear Dyn.*, 2016, **84**(2), p 437-472.
21. N. Langenbrunner, M. Weaver, M.G. Dunn, C. Padova, and J. Barton, Dynamic Response of a Metal and a CMC Turbine Blade During a Controlled Rub Event Using a Segmented Shroud, 2014.
22. R. Mandard, J.-F. Witz, X. Boidin, J. Fabis, Y. Desplanques and J. Meriaux, Interacting Force Estimation during Blade/Seal Rubs, *Tribol. Int.*, 2015, **82**, p 504-513.
23. Noel Paul Hopkins, Abradable Coatings - From Black Art to Materials Science, (Swansea University), 2007.
24. B. Zhang, M. Marshall and R. Lewis, Investigating Al-Si Base Abradable Material Removal Mechanism with Axial Movement in Labyrinth Seal System, *Wear*, 2022, **510-511**, 204496.
25. Oerlikon Metco, Rapid Validation of Turbomachinery Abradable Systems Using Oerlikon Metco's Rub-Test Facility, *SF-0029.0-Abradable Testing*, 2020.
26. J. Stringer and M.B. Marshall, High Speed Wear Testing of an Abradable Coating, *Wear*, 2012, **294-295**, p 257-263.
27. W. Xue, S. Gao, D. Duan, J. Zhang, Y. Liu and S. Li, Effects of Blade Material Characteristics on the High-Speed Rubbing Behavior between Al-hBN Abradable Seal Coatings and Blades, *Wear*, 2018, **410-411**, p 25-33.
28. B. Martinet, A. Cappella, S. Philippon and C. Montebello, Effect of Temperature on Wear Mechanisms of an Aluminium - Based Abradable Coating for Aircraft Engines after a Dynamic Interaction with a Ti6Al4V Blade, *Wear*, 2020, **446-447**, 203202.
29. G. Sutter, S. Philippon and F. Garcin, Dynamic Analysis of the Interaction between an Abradable Material and a Titanium Alloy, *Wear*, 2006, **261**(5-6), p 686-692.
30. X. Ma and A. Matthews, Investigation of Abradable Seal Coating Performance Using Scratch Testing, *Surf. Coat. Technol.*, 2007, **202**(4-7), p 1214-1220.
31. M. Yi, J. He, B. Huang and H. Zhou, Friction and Wear Behaviour and Abradability of Abradable Seal Coating, *Wear*, 1999, **231**(1), p 47-53.
32. P. Stoyanov, A. Boyne and A. Ignatov, Tribological Characteristics of Co-Based Plasma Sprayed Coating in Extreme Conditions, *Results Surf. Interfaces*, 2021, **3**, 100007.
33. C. Delebarre, V. Wagner, J.Y. Paris, G. Desein, J. Denape and J. Gurt-Santanach, An Experimental Study of the High Speed Interaction between a Labyrinth Seal and an Abradable Coating in a Turbo-Engine Application, *Wear*, 2014, **316**(1-2), p 109-118.
34. H.I.H. Saravanamuttoo, Ed., Gas Turbine Theory, 6th ed, (Pearson Prentice Hall, Harlow, New York) 2009.
35. S.C. Kacker and U. Okapuu, A Mean Line Prediction Method for Axial Flow Turbine Efficiency, *J. Eng. Power*, 1982, **104**(1), p 111-119.
36. H. Moustapha and M.F. Zelesky, Eds., Axial and Radial Turbines, (White River Junction, Vt), Concepts NREC, 2003.
37. B. Zhang and M. Marshall, Investigating Material Removal Mechanism of Al-Si Base Abradable Coating in Labyrinth Seal System, *Wear*, 2019, **426-427**, p 239-249.
38. N. Fois, M. Watson, J. Stringer and M. Marshall, An Investigation of the Relationship between Wear and Contact Force for Abradable Materials, *Proc. Inst. Mech. Eng. Part J. J. Eng. Tribol.*, 2015, **229**(2), p 136-150.
39. A. Dadouche, M.J. Conlon, W. Dmochowski, B. Liko, and J.-P. Bedard, Experimental Evaluation of Abradable Seal Performance at High Temperature, *Volume 5: Structures and Dynamics, Parts A and B*, (Berlin, Germany), ASMEDC, 2017, p 143-150, <https://doi.org/10.1115/GT2008-51228>.
40. Kistler Group, Kistler LabAmp—Charge Amplifier and Data Acquisition for Multi-Channel Measurement, 2017, https://kistler-embedded.partcommunity.com/3d-cad-models/FileService/File/kistler/07_electronics/01_charge_amplifiers/01_laboratory/5167a_english.pdf. Accessed 17 June 2024.
41. Kistler Group, Triaxial Load Cells, Piezoelectric Force Transducers, 2024, <https://www.kistler.com/CA/en/cp/triaxial-load-cells-93x7-8c/P0000703>. Accessed 17 June 2024.
42. FLIR Systems, FLIR A320 Tempscreen (9 Hz), 2018, <https://www.itm.com/pdfs/cache/www.itm.com/48201-1201/datasheet/48201-1201-datasheet.pdf>. Accessed 17 June 2024.
43. ST-PMCI Programmable Single Axis Motion Controller, *Variometer webshop*, 2024, <https://variometer.hu/en/programmable-single-axis-motion-controller>. Accessed 17 June 2024.
44. A.M. Kharaev, RCh. Bazheva and A.A. Chaika, Composite Materials Based on Polycarbonate (Review), *Int. Polym. Sci. Technol.*, 2007, **34**(10), p 27-33.
45. S. Sadeghi Esfahlani, Ballistic Performance of Polycarbonate and Polymethyl Methacrylate under Normal and Inclined Dynamic Impacts, *Heliyon*, 2021, **7**(4), p 106856.
46. S.M. Walley, J.E. Field, P.W. Blair and A.J. Milford, The Effect of Temperature on the Impact Behaviour of Glass/Polycarbonate Laminates, *Int. J. Impact Eng*, 2004, **30**(1), p 31-53.
47. J. Radin and W. Goldsmith, Normal Projectile Penetration and Perforation of Layered Targets, *Int. J. Impact Eng*, 1988, **7**(2), p 229-259.
48. Photron, FASTCAM SA1.1 Hardware Manual, HSI, 2024, https://www.highspeedimaging.com/media/photron_manuals/FASTCAM_SA1_1&SA1_IRV_HW_Manual.pdf.
49. Kistler Group, Triaxial Accelerometer Family Type 8763B, 2024, <https://www.kistler.com/CA/en/cp/iepe-triaxial-accelerometers-8763b/P0000559>. Accessed 10 July 2024.
50. K. Bertuol, F. Rivadeneira, R. Nair, B. Barnett, C. Moreau, and P. Stoyanov, Influence of hBN on the Abradable Performance of AlSi-Based Coatings: Bridging the Gap Between Tribological Assessment and Abradability Testing, *Surf. Coat. Technol.*, 2024, <https://doi.org/10.1016/j.surfcoat.2024.131060>.
51. C. Bidmeshki, A.C. Liberati, A. Roy, A.I. Encalada, F.B. Ettouil, S.A. Alidokht, R.R. Chromik, C. Moreau and P. Stoyanov, Microstructural, Mechanical, and Tribological Evaluation of Cu-Al-Based Coatings Deposited by APS and HVOF, *J. Therm. Spray Technol.*, 2023, **32**(8), p 2321-2335.

52. B. Arendarchuck, K. Bertuol, F. Rivadeneira, B. Castilho, B. Barnett, C. Moreau, and P. Stoyanov, Unveiling the Influence of Nickel on Erosion and Tribological Performance of AlSi-Based Abradable Coatings, (Submitted to Journal of Materials Science), 2024.
53. M. Watson, N. Fois and M.B. Marshall, Effects of Blade Surface Treatments in Tip-Shroud Abradable Contacts, *Wear*, 2015, **338-339**, p 268-281.
54. M. Watson and M. Marshall, Wear Mechanisms at the Blade Tip Seal Interface, *Wear*, 2018, **404-405**, p 176-193.
55. J. Liu, Y. Yu, T. Liu, X. Cheng, J. Shen and C. Li, The Influence of Composition and Microstructure on the Abradability of Aluminum-Based Abradable Coatings, *J. Therm. Spray Technol.*, 2017, **26**(6), p 1095-1103.
56. A. Wu, Z. Song, K. Nakata, J. Liao and L. Zhou, Interface and Properties of the Friction Stir Welded Joints of Titanium Alloy Ti6Al4V with Aluminum Alloy 6061, *Mater. Des.*, 2015, **71**, p 85-92.
57. J. Tang, F. Yu, H. Zhang and D. Chen, Effect of Microstructure Refining on the Thermal Stability and Wear Resistance of Abradable AlSi-Polyester Coating, *J. Therm. Spray Technol.*, 2021, **30**(6), p 1615-1623.
58. Z. Mutasim, L. Hsu, and E. Wong, Evaluation of Plasma Sprayed Abradable Coatings, 1992.
59. N. Fois, J. Stringer and M.B. Marshall, Adhesive Transfer in Aero-Engine Abradable Linings Contact, *Wear*, 2013, **304**(1-2), p 202-210.
60. E. Rahimov, M. Watson, A. Hadjisoteriou and M. Marshall, Investigation of Wear Mechanisms in AlSi-Polyester Abradable-Ti(6Al4V) Blade Contacts Using Stroboscopic Imaging, *Wear*, 2022, **494-495**, 204207.

Publisher's Note Springer Nature remains neutral with regard to jurisdictional claims in published maps and institutional affiliations.

Springer Nature or its licensor (e.g. a society or other partner) holds exclusive rights to this article under a publishing agreement with the author(s) or other rightsholder(s); author self-archiving of the accepted manuscript version of this article is solely governed by the terms of such publishing agreement and applicable law.